Intermolecular Coulombic Decay in Endohedral Fullerene at the $4d \rightarrow 4f$ Resonance

Razib Obaid,[1,*] Hui Xiong,[1] Sven Augustin,[2,3] Kirsten Schnorr,[2] Utuq Ablikim,[3] Andrea Battistoni,[4] Thomas J. A. Wolf,[4] René C. Bilodeau,[1] Timur Osipov,[5] Kirill Gokhberg,[6] Daniel Rolles,[3] Aaron C. LaForge,[1] and Nora Berrah[1]

[1]*Department of Physics, University of Connecticut, Storrs, Connecticut 06269, USA*
[2]*Max-Planck-Institut für Kernphysik, Heidelberg 69117, Germany*
[3]*J. R. Macdonald Laboratory, Physics Department, Kansas State University, Manhattan, Kansas 66506, USA*
[4]*PULSE Institute, SLAC National Accelerator Laboratory, 2575, Sand Hill Road, Menlo Park, California 94025, USA*
[5]*LCLS, SLAC National Accelerator Laboratory, 2575, Sand Hill Road, Menlo Park, California 94025, USA*
[6]*Theoretische Chemie, Physikalisch-Chemisches Institut, Universität Heidelberg, Heidelberg 69120, Germany*

(Received 3 September 2019; accepted 8 February 2020; published 17 March 2020)

Intermolecular processes offer unique decay mechanisms for complex systems to internally relax. Here, we report the observation of an intermolecular Coulombic decay channel in an endohedral fullerene, a holmium nitride complex (Ho_3N) embedded within a C_{80} fullerene, between neighboring holmium ions, and between the holmium complex and the carbon cage. By measuring the ions and the electrons in coincidence after XUV photoabsorption, we can isolate the different decay channels, which are found to be more prevalent relative to intra-atomic Auger decay.

DOI: 10.1103/PhysRevLett.124.113002

Endohedral fullerenes are unique three-dimensional clusterlike molecular systems where atoms, molecules, or other smaller clusters can be confined within a hollow spherical carbon molecular cage (henceforth simply "cage"). Discovered around the same time as C_{60} [1], endohedral fullerenes with confined metal species [2,3] have received broad interest in the field of condensed matter physics (see reviews in Refs. [4,5] for details), as well as in molecular physics due to their unique ionization and fragmentation mechanisms upon single photon excitation [6–10]. In particular, lanthanide-containing endohedral fullerenes have been considered of interest as drug delivery systems due to being excellent radio tracers [11], and in the field of radio therapeutics due to the large number of electrons they are able to release [12].

Additionally, endohedral fullerenes are predicted to exhibit strong intermolecular decay channels [13] upon inner-shell ionization through intermolecular Coulombic decay (ICD) [14]; however, to date, it has not been experimentally verified. ICD is an energy transfer process in which a photoexcited atom relaxes by transferring its excess energy to a neighboring atom. In the XUV regime, the mechanism has been observed in a wide range of weakly bound systems specifically when intramolecular processes such as Auger decay are energetically forbidden. For reviews, see Refs. [15,16]. For shorter wavelength light where Auger decay becomes a competing process, ICD can still play a prominent role in cascade-type ionization processes [17–20]. In particular, such mechanisms could play a role in biological systems where electronic relaxation of and charge transfer to metal absorbers drives intermolecular decay causing and propagating radiation damage to the surrounding molecular framework [21]. In this regard, endohedral fullerenes can serve as model systems for observing complex intermolecular host-dopant interactions. Due to the presence of electron correlation in the excited states, ICD is expected to provide an efficient pathway for relaxation of the guest species via cage ionization, producing stable multiply-charged states of the parent molecule as predicted in [13].

In the present work, we report on the inner-shell ionization of gas-phase $Ho_3N@C_{80}$ complexes (where @ indicates that Ho_3N is contained within the C_{80} cage). We show that between the metal holmium ions and the C_{80} cage such relaxation pathway exists, and is primarily responsible for charged parent molecular complex. Schematics of the formation of doubly charged parent molecule through Auger and ICD decays are shown in Fig. 1. At photon energies above the $4d$ resonance threshold of Ho^{3+}, the carbon cage is effectively transparent, due to low photoabsorption cross sections [22], while the holmium atoms have a relatively large photoabsorption cross section. From the electron kinetic energy (eKE) distribution in coincidence with different parent and fragmented ions, we observed the signatures of the predicted ICD [13] between the holmium and the cage, and cascade Auger-ICD between the holmium ions. In particular, we observe that these processes occur with higher efficiency than individual Auger decay mechanisms in the formation of multiply charged $Ho_3N@C_{80}$.

The experiment was performed at the beam line 10.0.1 of the Advanced Light Source at Lawrence Berkeley National

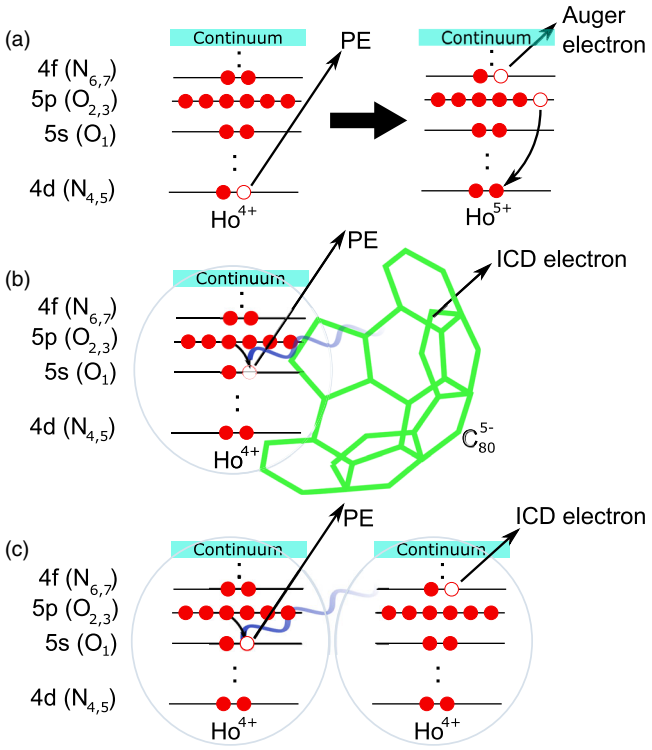

FIG. 1. The schematic of some exemplary ionization and ICD pathways to form $Ho_3N@C_{80}^{2+}$ are shown above. The binding energies of the orbitals shown are given in the Supplemental Material [23], Table 1. (a) The two-step process of photoionization, with the removal of a photoelectron (PE), and Auger decay ($N_{4,5}O_{2,3}N_{6,7}$) of a single Ho^{3+} to form Ho^{5+}. The ICD channels between holmium and the C_{80} cage, and between two holmium ions are given in (b) and (c), respectively.

Laboratory. We use ion-electron coincidence spectroscopy combined with the velocity-map imaging (VMI) technique [24], which measures the kinetic energy of the detected particles. The details of the double VMI spectrometer are described elsewhere [25]. For the present experiment, we evaporated $Ho_3N@C_{80}$ in its gas phase at about 900 K using an effusive oven giving a target density of $\sim 10^8$ cm^{-3}.

To form a stable complex, each holmium atom in the neutral $Ho_3N@C_{80}$ system donates 1 electron to the N and 2 electrons to the surrounding C_{80} cage, producing the following charge distribution: $(Ho^{3+})_3\ N^{3-}@C_{80}^{6-}$ [4,26]. The high Ho-N bonding energy prevents the formation of the complex without this effective 3-electron donation from each of the holmium atoms [27]. The resulting electronic configuration of Ho^{3+} ($4d^{10}5s^25p^64f^{10}$) has a partly filled $4f$ orbital. The large overlap between the $4d$ and $4f$ orbital wave functions leads to the appearance of atomiclike $4d^{10}\ 4f^{10} \rightarrow 4d^9\ 4f^{11}$ transitions in Ho^{3+}, which are characterized by large transition strengths and produce the so-called "giant resonance" [28] around 160 eV. In the molecular complex of $Ho_3N@C_{80}$, the distance between the two neighboring holmium ions in the equilibrium configuration is about 3.5 Å, and the separation between one of the holmium and the neighboring carbon atoms are estimated between 2 and 2.5 Å [29].

Figure 2 shows the eKE distributions obtained by VMI image reconstruction using pBasex [30] in coincidence with different charge states of the parent molecule, at different photoexcitation energies. 149.0 eV is below the $4d$ threshold of $Ho_3N@C_{80}$, and $h\nu = 156.9$ and $h\nu = 158.9$ eV are near, but below the $4d$ threshold and have $4f - 4f$ transitions in the holmium ions [28]. The photon energies of 163.3 and 168.8 eV are above the binding energy of the $4d$ orbitals of Ho^{3+} [31]. As discussed later, the signatures of ICD in $Ho_3N@C_{80}{}^{2+}$ and $Ho_3N@C_{80}{}^{3+}$ are present in Figs. 2(b) and 2(c), and shown in 2(e) and 2(f).

Figure 2(a) shows the eKE distribution in coincidence with $Ho_3N@C_{80}{}^{+}$. In this case, the endohedral fullerene is singly ionized, thus decay mechanisms (e.g., Auger, shake-off, and thermal [32]) resulting in higher charged states are naturally excluded. From the peak maximum at the different photon energies, it is clear that the peaks (i) are broad (about 40 eV FWHM for $h\nu = 168.8$ eV), and (ii) show characteristics of direct photoemission due to photon-energy dependent shifts. Electrons from direct photoionization of singly charged ions originate from $5s$ (binding energies, BE = 50.4, 52.6 eV), $5p$ ($5p_{1/2,3/2}$ BE = 32.5, 26.8 eV), and $4f$ ($4f_{5/2,7/2}$ BE = 11.1, 8.0 eV) [31] states of the Ho^{3+} atoms, or from the valence orbital of the cage (IP = 6.5 eV [33]). Additionally, as observed for other lanthanides [34–36] due to $4d - 4f$ Auger resonances, the intensity of the $5s$ and $5p$ electrons are known to be significantly enhanced.

In order to explain the distribution of the eKE spectra, we fit the distribution of $h\nu = 168.8$ eV with multiple Lorentzian functions, as shown in Fig. 2(d). Here, we show that, without overfitting the data, three peaks reproduce the eKE distribution with $R^2 = 0.981$. The peaks at 107.9 ± 4.2 eV (FWHM = 42.1 eV), 133.7 ± 0.9 eV (FWHM = 21.3 eV), and 147.3 ± 0.3 eV (FWHM = 13.8 eV) are identified as photoelectrons originating from the $5s$, the $5p_{1/2}$, and a combination of peaks from $5p_{3/2}$, $4f$, and the cage, respectively. As observed in Figs. 2(a) and 2(d), the broadening of the photoelectron peaks is due to a fast decay via vibronic coupling which follows from other highly excited states being populated so that no secondary electrons are emitted [37–39].

Figures 2(b) and 2(c) show the eKE distributions in coincidence with the $Ho_3N@C_{80}{}^{2+}$ and $Ho_3N@C_{80}{}^{3+}$, respectively. In this case, the electron distributions can originate from autoionization mechanisms which were excluded for the case of $Ho_3N@C_{80}{}^{+}$. To better understand the multitude of electron distributions for $Ho_3N@C_{80}{}^{2+}$, we focus our discussion on $h\nu = 168.8$ eV. As done previously, we fit our data with another set of multiple Lorentzian functions as shown in Fig. 2(e) (other eKE distributions and the corresponding fit for different photon

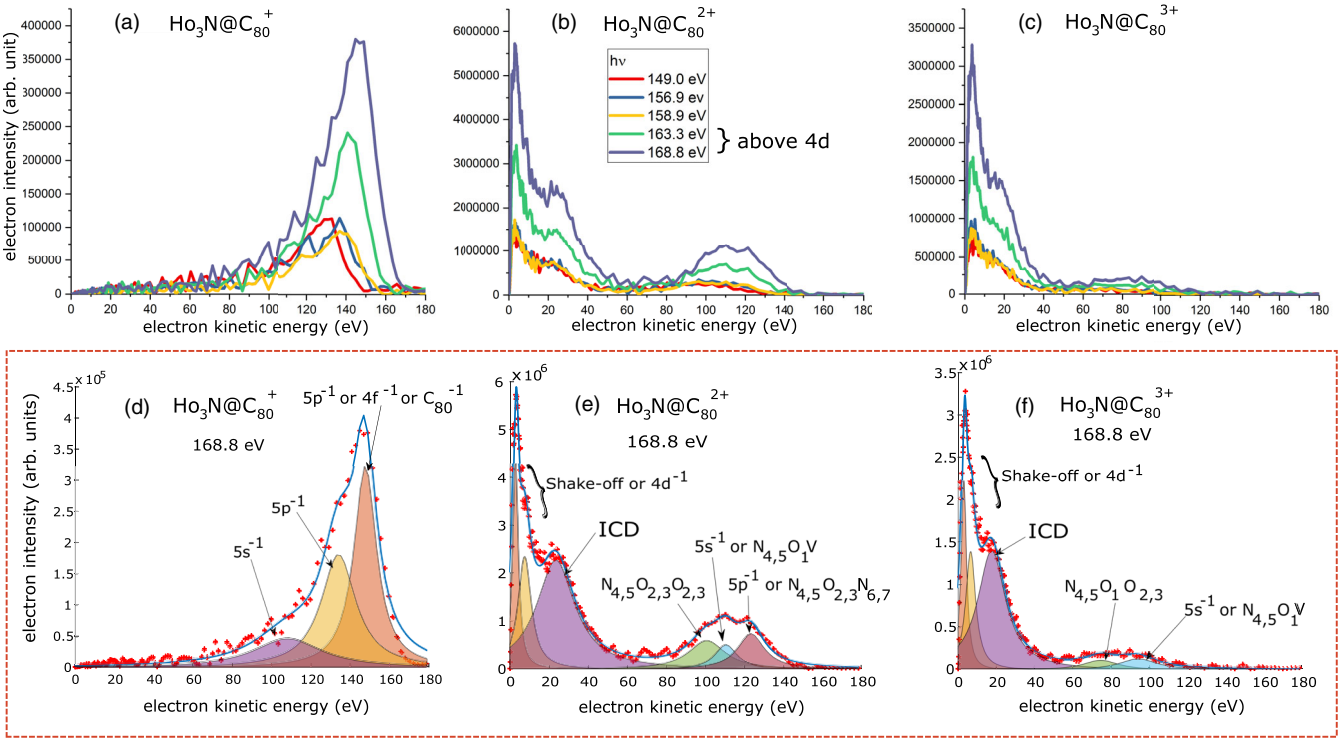

FIG. 2. The electron kinetic energy (eKE) distributions at different photon energies, in coincidence with various charge states of the parent molecule [plots (a),(b), and (c)] for photon energies below and above the $4d$ threshold. (d),(e), and (f) The fitted data for electrons detected in coincidence with $Ho_3N@C_{80}^{+}$ (top), $Ho_3N@C_{80}^{2+}$ (middle), and $Ho_3N@C_{80}^{3+}$ (bottom) at a photon energy of 168.8 eV. Lorentz functions, $y = y_0 + (2A/\pi)\{w/[4(x - x_c)^2 + w^2]\}$ are used to fit the peaks, where w, x_c, and A are the full-width at half maximum (FWHM), the center, and the area, respectively.

energies can be found in the Supplemental Material Figs. 2 and 3). Altogether six Lorentzian peaks reproduce the eKE distributions at $h\nu = 168.8$ eV, with $R^2 = 0.961$. The peak with kinetic energy around 123.1 ± 5.0 eV (FWHM = 16.6 eV) corresponds to direct Auger decay of holmium ion initiated by the removal of a $4d$ electron followed by $4d^9 5p^6 4f^{10} \rightarrow 4d^{10} 5p^5 4f^9 + e^-$ ($N_{4,5}O_{2,3}N_{6,7}$). At the $4d \rightarrow 4f$ photon energy or below, a resonant Auger decay ensues from the excitation to $4f$ orbitals in the form of $4d^9 5p^6 4f^{11} \rightarrow 4d^{10} 5p^5 4f^9 + 2e^-$ ($N_{4,5}O_{2,3}N_{6,7}$). This peak resulting from the local Auger decay in Ho^{3+} was previously observed in elemental holmium [40], and is shown in the schematic of Fig. 1(a). The electron kinetic energy in the Auger decay is calculated by: $E_k = E_A - E_B - E_C - U_{\mathrm{eff(BC)}}$, where $U_{\mathrm{eff(BC)}}$ is the Coulomb interaction between the two vacancies in the final state, and E_A, E_B, E_C are the binding energies of the three participating electrons (see Supplemental Material [23] Table 1). For the case of Ho^{3+}, $U_{\mathrm{eff(BC)}}$ is between 1.5 and 6 eV [40]. In addition to the Auger decay, photoionization of $5p$ electrons of Ho^{3+} (eKE: 136–142 eV at $h\nu = 168.8$ eV) (Supplemental Material [23], Table 1) also gives rise to this peak.

The neighboring peak centered around 110.3 ± 6.8 eV (FWHM = 13.6 eV) originates from another direct Auger transitions of the form of $N_{4,5}O_1V$, where V is the valence orbital of the cage. At photon energies below or at the $4d \rightarrow 4f$, the resonant Auger process is again initiated by the excitation to a $4f$ state in the form of $4d^9 5s^2 4f^{11} V \rightarrow 4d^{10} 5s^1 4f^{11} V^{-1} + 2e^-$ ($N_{4,5}O_1V$). Interestingly, the Auger decay of $N_{4,5}O_1V$ is not detected in metal holmium photoemission spectra [40], but is prominent in $Ho_3N@C_{80}$ due to the presence of excess valence electrons from the carbon cage, as well as three additional electrons from the center nitrogen atom. Additionally, the photoionization of a $5s$ electron (BE = 50.4, 52.6 eV) can also contribute to this peak. Note that photoionization of $5p/5s$ would also have to have an additional step where a second electron is emitted.

The next peak at around 100.6 ± 14.7 eV (FWHM = 22.6 eV) arises due to the removal of a $4d$ electrons, contributing to the low kinetic energy electrons in ekE spectrum. The $4d$ hole eventually decays by producing a Coster-Kronig type transition where two electrons from the $5p$ orbitals participate to form the Auger decay of $N_{4,5}O_{2,3}O_{2,3}$, as was also observed in Refs. [40,41]. Near the $4d \rightarrow 4f$, the peak originates from $4d^9 4f^{11}$ excited state, where the excited $4d$ electron acts as a spectator. Since, in the $4d \rightarrow 4f$ resonance, there exists resonant enhancement of the $5p$ photoabsorption cross sections for

lanthanides [34–36,42,43], the resonantly excited $4d$ electron eventually decays by producing the Coster-Kronig transition of $N_{4,5}O_{2,3}O_{2,3}$. The formerly spectator $4d$ electron then undergoes tunneling and is detected as a low kinetic energies [44] shake-off electron. The low kinetic energy electron peaks between 0 and 8 eV are the photoelectrons from $4d$ ionization or those following shake-off of the spectator $4d$ electron participating in the $4d^9 4f^{11}$ excited state as discussed earlier for the case of the resonant Auger decay of $N_{4,5}O_{2,3}O_{2,3}$ or $N_{4,5}O_1V$.

We attribute the large peak at 23.8 ± 0.8 eV (FWHM = 23.7 eV) to ICD, which follows from the photoionization of the resonantly enhanced $5s$ and $5p$ orbitals of one of the three Ho^{3+} at or around the $4d \rightarrow 4f$. The eKE from the $5s$ and $5p$ vacancies are similar to the one for the $N_{4,5}O_1V$ and $N_{4,5}O_{2,3}O_{2,3}$ decays, and thus the peaks from these should appear superimposed with the peaks at 110 and 123 eV. Following this initial step, the states then either decay with the cage (eKE: 20–47 eV) or with another holmium (eKE: 14–45 eV) as shown in Eqs. (1) and (2). The expected peak positions of the ICD were calculated from the energy difference between the orbitals of holmium ions with initial $5p$ and $5s$ vacancies, followed by the $4f$ orbital vacancy created in one of the neighboring holmium ions, or the valence orbital of the cage at the ICD step. Without this ICD step, the electron kinetic energy distribution is not expected to show any peak in this energy range, as previously calculated and measured for lanthanides [45,46]. To our knowledge, there are no other mechanisms that can give rise to electrons in this kinetic energy range for photo-excitation between $h\nu = 149$ and $h\nu = 170$ eV. Following the ICD step, an electronically stable doubly charged parent molecular complex is formed. Otherwise, an additional decay step will ensure formation of a triply charged complex. Additionally, the ICD of these states competes with the nonadiabatic decay we discussed in relation to the $Ho_3N@C_{80}{}^+$ spectrum. The presence of the $5p$ photoelectrons in the latter and the ICD peak in the current spectrum indicate that the vibrational relaxation and the ICD have comparable decay rates.

$$Ho^{4+*}(5s^{-1}/5p^{-1})C_{80}^{6-} \xrightarrow{\text{ICD}} Ho^{4+}C_{80}^{5-} + e^- \qquad (1)$$

$$Ho^{4+*}(5s^{-1}/5p^{-1})Ho^{3+} \xrightarrow{\text{ICD}} Ho^{4+}Ho^{4+} + e^- \qquad (2)$$

The ICD pathways are also prominent for the eKE distributions in coincidence with $Ho_3N@C_{80}{}^{3+}$, as seen in Fig. 2(c) [also Fig. 2(f) for $h\nu = 168.8$ eV]. Here also the shake-off and autoionization states below 10 eV are dominant channels as was the case for the eKE distributions for $Ho_3N@C_{80}{}^{2+}$ as discussed above. Only now, the $5p^{-1}$ decays further through the $4f^{-1}$ cascade removing an additional electron with kinetic energy between 3 and 6 eV, as is seen in Fig. 2(f). Furthermore, a weak yield is observed for electron kinetic energies between 60 and 120 eV due to Auger decay from $N_{4,5}O_1O_{2,3}$ and $N_{4,5}O_1V$. However, the most prominent decay channels are seen to be cascade decay from the $5p^{-1}4f^{-1}$ states of one of the holmium ions forming Ho^{5+} followed by the emission of an electron from a neighboring Ho^{3+} (with the $4f^{-1}$ state initiating an Auger-ICD cascade). A detailed schematic of this process is shown in the Supplemental Material [23], Fig. 5. Instead of the neighboring Ho^{3+} with its $4f^{-1}$ state, the cage can also participate with its valence electrons, yielding electron with kinetic energies from a few eV to 25 eV.

For the case of producing both $Ho_3N@C_{80}{}^{2+}$ and $Ho_3N@C_{80}{}^{3+}$ by multiply ionizing the holmium ions, we observe that the ICD process is more prevalent over individual local Auger decay processes. In some non-endohedral covalently bonded system such as XeF_n, the expected decrease in Auger linewidth with increasing number of fluorine atoms (n) [47] is not observed due to strong intermolecular decay [48]. However, such observation of ICD processes being more efficient compared to Auger decay in endohedral system has not been previously made. Additionally, the multiply charged states of the parent molecule are also stable in terms of fragmentation. This was also previously predicted in Ref. [13] for $Ne@C_{60}$, since the stability is ensured by the higher cage dissociation energy [49] following the inclusion of the inner species undergoing ICD. Far below the $4d$ threshold, at $h\nu = 149.0$ eV, $Ho_3N@C_{80}{}^{3+}$ can be produced by an ICD-ICD cascade, as was discussed in Ref. [13]. This is a two-step process, in which the first step is initiated by a $5s$ vacancy in one of the holmium site filled by a $5p$ electron, while an electron is emitted from a neighbor, such as another Ho^{3+} or the cage. In the second step, the $5p$ vacancy in the original holmium ion is filled by a $4f$ electron causing the emission of an ICD electron from the same holmium ion. Supplemental Material [23], Fig. 6 shows an illustrative stepwise schematics of the ICD-ICD cascade. The stepwise relaxation of $5s$ vacancy on Ho^{3+} can also be accompanied by the emission of ICD electrons from the C_{80} cage. The expected eKE for this process is between 14 and 22 eV.

To further explore any photon energy dependence of the ICD electrons originating from the different species, we also examined the ICD peak positions. Figure 3 shows the different ICD peaks extracted from the Lorentzian fitting of the eKE distribution for different photon energies. The ICD peak width for $Ho_3N@C_{80}{}^{2+}$ and $Ho_3N@C_{80}{}^{3+}$ are about 23.96 ± 0.75 and 17.34 ± 0.92 eV, respectively. The ICD eKE distributions for $Ho_3N@C_{80}{}^{2+}$ is centered around 23 eV for photon energies between 158.9 and 168.8 eV, while for $h\nu = 149.0$ eV, it is around 18 eV, indicating that the mechanism involves photoionization of the $5p_{1/2}$ (BE = 32.5 eV) and $5p_{3/2}$ (BE = 26.8 eV) orbitals in the first step. From Refs. [40,43], it is known that below

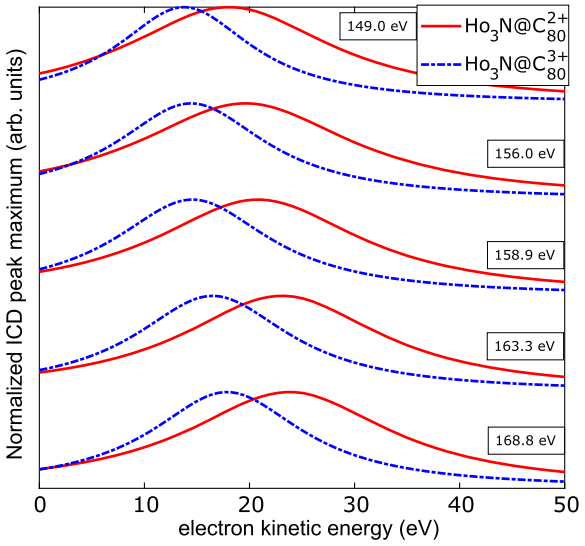

FIG. 3. The ICD peaks for different charge states for different photon energies normalized by the individual ICD peak maximum.

the $4d-4f$ resonance, the $5p_{1/2}$ cross section is smaller than the $5p_{3/2}$. Across the resonance, they become of similar strength. Additionally, an ICD electron originating from the decay of the $5p_{1/2}$ state should have higher kinetic energies. This, together with the increasing contribution of the $5p_{1/2}$ state as the photon energy is increased, shifts the ICD peak to higher energies. For $Ho_3N@C_{80}{}^{3+}$, the peak position around $4d$ excitation is about 16 eV, while for 149.0 eV, the peak lies around 14 eV, supporting the mechanisms Auger-ICD and ICD-ICD cascade for the different photon energies.

In conclusion, we have observed intermolecular Coulombic decay in endohedral fullerene, $Ho_3N@C_{80}$, through the use of coincident ion-electron spectroscopy. We have shown that these ICD processes, subsequent to inner-shell ionization, are much stronger than local, intra-atomic Auger decay by forming multiple charge states of $(Ho^{3+})_3\ N^{3-}@C_{80}{}^{6-}$ around the $4d \rightarrow 4f$ transitions. Furthermore, we observed the dominance of $5s/5p$ photoelectron lines in the $Ho_3N@C_{80}{}^{+}$ spectrum. Because of the $4d-4f$ resonance, the $5s/5p$ orbitals are resonantly enhanced, opening the ICD channels at around 30 eV. Additionally, cascade type ICD also plays an important role in the formation of triply charged complexes. These cascade processes warrant further investigation at higher x-ray photon energies for metal-cage complexes, which can act as a prototypical system to study radiation induced damage in the high-intensity regime accessed by free-electron lasers.

We sincerely thank the staff of the Advanced Light Source for their help and hospitality during the beam time. This work was funded by the Department of Energy, Office of Science, Basic Energy Sciences (BES), Division of Chemical Sciences, Geosciences, and Biosciences (PULSE group), and under Grant No. DE-SC0012376 (UConn Group) and DE-FG02-86ER13491 (Kansas State Group). Financial support for theoretical work by the European Research Council (ERC) (Advanced Investigator Grant No. 692657) is gratefully acknowledged (K. G.). We thank L. S. Cederbaum for helpful discussions.

*razib.obaid@uconn.edu

[1] H. W. Kroto, J. R. Heath, S. C. O'Brien, R. F. Curl, and R. E. Smalley, Nature (London) **318**, 162 (1985).
[2] J. Heath, S. O'brien, Q. Zhang, Y. Liu, R. Curl, F. Tittel, and R. Smalley, J. Am. Chem. Soc. **107**, 7779 (1985).
[3] H. Shinohara, H. Yamaguchi, N. Hayashi, H. Sato, M. Ohkohchi, Y. Ando, and Y. Saito, J. Phys. Chem. **97**, 4259 (1993).
[4] A. A. Popov, S. Yang, and L. Dunsch, Chem. Rev. **113**, 5989 (2013).
[5] A. Rodríguez-Fortea, A. L. Balch, and J. M. Poblet, Chem. Soc. Rev. **40**, 3551 (2011).
[6] A. Müller, S. Schippers, R. Phaneuf, M. Habibi, D. Esteves, J. Wang, A. Kilcoyne, A. Aguilar, S. Yang, and L. Dunsch, J. Phys. Conf. Ser. **88**, 012038 (2007).
[7] A. L. D. Kilcoyne, A. Aguilar, A. Müller, S. Schippers, C. Cisneros, G. Alna Washi, N. B. Aryal, K. K. Baral, D. A. Esteves, C. M. Thomas, and R. A. Phaneuf, Phys. Rev. Lett. **105**, 213001 (2010).
[8] H. Xiong, R. Obaid, L. Fang, C. Bomme, N. G. Kling, U. Ablikim, V. Petrovic, C. E. Liekhus-Schmaltz, H. Li, R. C. Bilodeau *et al.*, Phys. Rev. A **96**, 033408 (2017).
[9] A. Müller, M. Martins, A. L. D. Kilcoyne, R. A. Phaneuf, J. Hellhund, A. Borovik, Jr., K. Holste, S. Bari, T. Buhr, S. Klumpp *et al.*, Phys. Rev. A **99**, 063401 (2019).
[10] R. Obaid, K. Schnorr, T. J. Wolf, T. Takanashi, N. G. Kling, K. Kooser, K. Nagaya, S.-i. Wada, L. Fang, S. Augustin *et al.*, J. Chem. Phys. **151**, 104308 (2019).
[11] D. W. Cagle, S. J. Kennel, S. Mirzadeh, J. M. Alford, and L. J. Wilson, Proc. Natl. Acad. Sci. U.S. A. **96**, 5182 (1999).
[12] Z. Kuncic and S. Lacombe, Phys. Med. Biol. **63**, 02TR01 (2018).
[13] V. Averbukh and L. S. Cederbaum, Phys. Rev. Lett. **96**, 053401 (2006).
[14] L. S. Cederbaum, J. Zobeley, and F. Tarantelli, Phys. Rev. Lett. **79**, 4778 (1997).
[15] T. Jahnke, J. Phys. B **48**, 082001 (2015).
[16] U. Hergenhahn, J. Electron Spectrosc. Relat. Phenom. **184**, 78 (2011).
[17] K. Gokhberg, P. Kolorenč, A. I. Kuleff, and L. S. Cederbaum, Nature (London) **505**, 661 (2014).
[18] F. Trinter, M. Schöffler, H.-K. Kim, F. Sturm, K. Cole, N. Neumann, A. Vredenborg, J. Williams, I. Bocharova, R. Guillemin *et al.*, Nature (London) **505**, 664 (2014).
[19] Y. Morishita, X.-J. Liu, N. Saito, T. Lischke, M. Kato, G. Prümper, M. Oura, H. Yamaoka, Y. Tamenori, I. H. Suzuki, and K. Ueda, Phys. Rev. Lett. **96**, 243402 (2006).
[20] R. Santra and L. S. Cederbaum, Phys. Rev. Lett. **90**, 153401 (2003).

[21] V. Stumpf, K. Gokhberg, and L. S. Cederbaum, Nat. Chem. **8**, 237 (2016).
[22] B. L. Henke, E. M. Gullikson, and J. C. Davis, At. Data Nucl. Data Tables **54**, 181 (1993).
[23] See Supplemental Material at http://link.aps.org/supplemental/10.1103/PhysRevLett.124.113002 for binding energies of the Holmium ions, additional fittings of the peaks for different ions at different photo-excitation energies, and the schematic of ICD pathways to form triply ionized parent molecule.
[24] A. T. Eppink and D. H. Parker, Rev. Sci. Instrum. **68**, 3477 (1997).
[25] U. Ablikim, C. Bomme, T. Osipov, H. Xiong, R. Obaid, R. C. Bilodeau, N. G. Kling, I. Dumitriu, S. Augustin, S. Pathak *et al.*, Rev. Sci. Instrum. **90**, 055103 (2019).
[26] M. Wolf, K.-H. Müller, D. Eckert, Y. Skourski, P. Georgi, R. Marczak, M. Krause, and L. Dunsch, J. Magn. Magn. Mater. **290**, 290 (2005).
[27] A. A. Popov and L. Dunsch, J. Am. Chem. Soc. **129**, 11835 (2007).
[28] J. P. Connerade, J. M. Estava, and R. C. Karnatak, in *Giant Resonances in Atoms, Molecules, and Solids*, NATO ASI Series: Physics Vol. 151 (Plenum Press, New York, 1987).
[29] A. A. Popov, *Endohedral Fullerenes: Electron Transfer and Spin* (Springer, Cham, 2017).
[30] G. A. Garcia, L. Nahon, and I. Powis, Rev. Sci. Instrum. **75**, 4989 (2004).
[31] B. Padalia, W. C. Lang, P. Norris, L. Watson, and D. Fabian, Proc. R. Soc. A **354**, 269 (1977).
[32] K. Hansen, R. Richter, M. Alagia, S. Stranges, L. Schio, P. Salén, V. Yatsyna, R. Feifel, and V. Zhaunerchyk, Phys. Rev. Lett. **118**, 103001 (2017).
[33] H. Xiong, B. Mignolet, L. Fang, T. Osipov, T. J. Wolf, E. Sistrunk, M. Gühr, F. Remacle, and N. Berrah, Sci. Rep. **7**, 121 (2017).
[34] O.-P. Sairanen, S. Aksela, and A. Kivimaki, J. Phys. Condens. Matter **3**, 8707 (1991).
[35] O.-P. Sairanen and S. Aksela, J. Phys. Condens. Matter **4**, 3337 (1992).
[36] K. Ichikawa, O. Aita, K. Aoki, M. Kamada, and K. Tsutsumi, Phys. Rev. B **45**, 3221 (1992).
[37] A. Marciniak, V. Despré, V. Loriot, G. Karras, M. Hervé, L. Quintard, F. Catoire, C. Joblin, E. Constant, A. Kuleff *et al.*, Nat. Commun. **10**, 337 (2019).
[38] A. J. Marks and K. Prassides, J. Chem. Phys. **98**, 4805 (1993).
[39] F. Lepine, B. Baguenard, B. Concina, M.-A. Lebeault, and C. Bordas, Mol. Phys. **105**, 1631 (2007).
[40] J. Riviere, F. Netzer, G. Rosina, G. Strasser, and J. Matthew, J. Electron Spectrosc. Relat. Phenom. **36**, 331 (1985).
[41] O.-P. Sairanen and S. Aksela, J. Phys. Condens. Matter **4**, 9213 (1992).
[42] W. F. Egelhoff, Jr., G. G. Tibbetts, M. H. Hecht, and I. Lindau, Phys. Rev. Lett. **46**, 1071 (1981).
[43] M. Aono, T.-C. Chiang, J. A. Knapp, T. Tanaka, and D. E. Eastman, Phys. Rev. B **21**, 2661 (1980).
[44] P. Linusson, S. Fritzsche, J. H. D. Eland, L. Hedin, L. Karlsson, and R. Feifel, Phys. Rev. A **83**, 023424 (2011).
[45] A. Kochur, V. Sukhorukov, and I. Petrov, J. Phys. B **29**, 4565 (1996).
[46] A. Sankari, R. Sankari, S. Heinäsmäki, M. Huttula, S. Aksela, and H. Aksela, Phys. Rev. A **77**, 052703 (2008).
[47] J. Cutler, G. Bancroft, J. Bozek, K. Tan, and G. Schrobilgen, J. Am. Chem. Soc. **113**, 9125 (1991).
[48] C. Buth, R. Santra, and L. S. Cederbaum, J. Chem. Phys. **119**, 10575 (2003).
[49] S. Tomita, J. U. Andersen, C. Gottrup, P. Hvelplund, and U. V. Pedersen, Phys. Rev. Lett. **87**, 073401 (2001).